Leapfrogging criteria for a line vortex pair external to a circular cylinder

by M.R. Turner[1]

Department of Mathematics, University of Surrey,
Guildford, Surrey GU2 7XH, UK

– Abstract –

The interaction of two line vortices of differing strengths in the presence of a circular cylinder is considered. An explicit criteria is derived, a function of the vortex strengths (including strengths of opposite sign) and the cylinder radius, which separates different behaviours of the system. If the initial position of the vortices satisfy this criteria, they will undergo a periodic leapfrogging motion as they rotate around the cylinder, otherwise the vortices still interact weakly with one another except without leapfrogging. This is in contrast to the planar wall case where if no periodic leapfrogging occurs then the vortices move apart and do not interact with each other. Numerical results for initial vortex positions which do, and do not satisfy this criteria are presented to demonstrate the different motions available, as well as the robustness of the criteria.

— March 18, 2021—

Keywords: leapfrogging; vortex; overtake; circular cylinder

1 Introduction

In an inviscid fluid, examining the motion and interaction of line vortices in the horizontal plane is a rich and well studied problem, reaching all the way back to the work of Helmholtz [1] (translated by [2]). Since then there have been notable studies on the so-called N-*vortex problem*, due to the fact that the governing equations have a simple structure, yet the possible motions which they contain is vast. For $N = 1$, 2 and 3 vortices the system is integrable and so the system exhibits predictable dynamics. For example, for $N = 2$ the vortices can rotate about a point or travel along a common axis as pair, if the absolute values of their strengths are equal, while for $N = 3$ the array of motions is richer, but still contains both bounded and unbounded motions [3, 4, 5]. For $N \geq 4$ the system is typically chaotic, unless some prescribed symmetry is imposed on the vortices. For more

[1]m.turner@surrey.ac.uk

information on the historical aspect of the N-vortex problem the reader is referred to [6] and [5] and the references therein.

The $N = 4$ planar vortex case, where the vortices come in pairs of equal and opposite strength either side of a common axis, is often used as a simple model to study the interaction of three-dimensional vortex rings. The interaction of two vortex rings has received experimental, numerical and theoretical treatment over the years, most notably because the rings can undergo a leapfrogging motion [7, 8, 9, 10, 11, 12, 13]. This is when the trailing ring shrinks and accelerates, while the leading ring expands and decelerates causing the faster trailing ring to pass through the leading ring. This process then repeats periodically. The planar $N = 4$ line vortex model also demonstrates this behaviour and is typically studied using four vortices with equal absolute strengths [14, 15, 16, 17, 5]. The case of leapfrogging for different strength vortex pairs was considered in [18], who identified a full description of the possible motions of two vortex rings for a wide range of initial conditions, as well as in [19] who derived an explicit criteria for the generation of leapfrogging in the planar problem. This criteria is a function of the vortex strength ratio and the initial separation of the vortices.

Using the method of images [20], the $N = 4$ planar vortex problem above with this symmetry also represents the flow for two interacting vortices next to an impermeable barrier, which is of interest in this work. In the world's oceans, vortices typically have long lifetimes and thus can propagate large distances via background currents or via the planetary vorticity gradient [21]. In doing so many will encounter topological barriers including coastlines [22, 23, 24] or seamounts [25, 26], and as these vortices transport significant amounts of heat, momentum, mass and salt in the world's oceans, understanding their motion close to, and interaction with, these barriers is important. In this work we investigate the interaction of two vortices with the coastline of a circular island, and in particular we identify a criteria for the periodic leapfrogging motion of these vortices, using an approach similar to [19].

We consider a simplified model of the full vortex/island interaction problem consisting of a pair of line vortices in an inviscid, irrotational fluid external to a circular cylinder. The results in this simplified model will help to inform results from simulations of the fully viscous Navier-Stokes equations which address the full problem. The case of a single line vortex external to a circular cylinder is straightforward and exhibits circular motion at a fixed distance from the barrier [27]. Here the vortex motion is in fact due to the induced velocity of two image vortices inside the cylinder. In this work we consider two vortices of different strengths, Γ_1 and Γ_2 (including cases of opposite sign) and find that leapfrogging motion is possible for all combinations of $0 < |\Gamma_1/\Gamma_2| \leq 1$, with $\Gamma_1 + \Gamma_2 \neq 0$, for all cylinder radii, a, but in many cases it is required that the vortices be initialized very close to each other. Leapfrogging does not occur for the case $\Gamma_1 + \Gamma_2 = 0$ as the vortices cannot swap their radial order with respect to the cylinder.

The current paper is laid out as follows. In 2.1 we formulate the governing ODEs from the complex potential and confirm the system is Hamiltonian, while in 2.2 we derive the criteria for the existence of leapfrogging vortices. In 3 we illustrate the leapfrogging motion by integrating the governing ODEs, and demonstrate the robustness of the existence criteria. Conclusions and future extensions are discussed in 4.

2 Formulation

2.1 Derivation of Governing Equations

We consider two line vortices in an inviscid, irrotational fluid which fills the two-dimensional z-plane exterior to an impermeable circular cylinder of radius a, centred on the origin. The vortices, labelled vortex 1 and vortex 2, have strengths Γ_j and lie at $z = z_j$ for $j = 1, 2$ with $|z_j| > a$. A schematic diagram for the problem setup can be found in figure 1, where we write $z = re^{\mathrm{i}\theta}$ with (r, θ) the usual plane polar coordinates and $\mathrm{i} = \sqrt{-1}$. We consider the situation where $0 < |\Gamma_2| \leq \Gamma_1$, excluding the case $\Gamma_1 + \Gamma_2 = 0$, and note

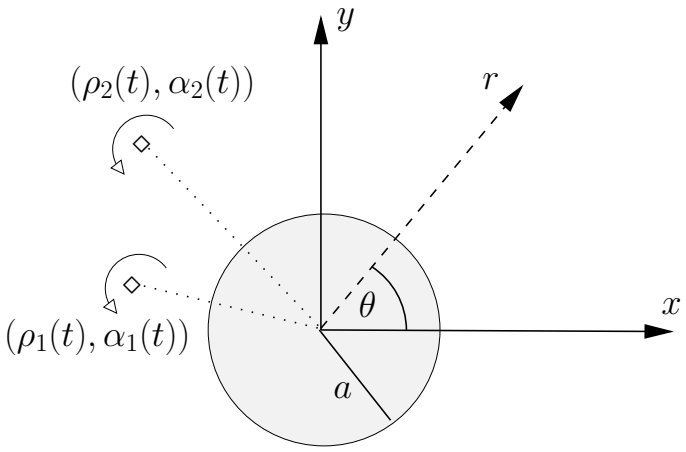

Figure 1: Schematic setup of two line vortices outside of a circular cylinder of radius a. The vortices have strengths Γ_j and are located at the polar coordinates $(\rho_j(t), \alpha_j(t))$ for $j = 1, 2$.

that the case $\Gamma_1 < |\Gamma_2|$ leads to identical results.

The complex potential for the flow around the cylinder can be written down using the Milne-Thomson circle theorem [27] as

$$w(z) = -\frac{\mathrm{i}\Gamma_1}{2\pi}\log(z-z_1) - \frac{\mathrm{i}\Gamma_2}{2\pi}\log(z-z_2) + \frac{\mathrm{i}\Gamma_1}{2\pi}\log\left(\frac{z\overline{z}_1 - a^2}{z}\right) + \frac{\mathrm{i}\Gamma_2}{2\pi}\log\left(\frac{z\overline{z}_2 - a^2}{z}\right), \quad (1)$$

where the overbar signifies the complex conjugate, and we have neglected any additive constant without loss of generality. Thus by noting that

$$\frac{\mathrm{i}\Gamma_j}{2\pi}\log\left(\frac{z\overline{z}_j - a^2}{z}\right) = \frac{\mathrm{i}\Gamma_j}{2\pi}\left[\log\left(z - \frac{a^2}{\overline{z}_j}\right) - \log(z) + \log(\overline{z}_j)\right],$$

for $j = 1, 2$ the flow external to the cylinder actually consists of a flow generated by the two physical vortices together with four additional image vortices which lie in $|z| < a$. By writing the time-dependent position of the physical vortices as

$$z_j(t) = \rho_j(t)e^{\mathrm{i}\alpha_j(t)},$$

and noting that the streamfunction for the flow is given by $\psi(r, \theta; \rho_1, \alpha_1, \rho_2, \alpha_2) = \mathrm{Im}(w)$

then

$$\begin{aligned}\psi(r,\theta) &= -\frac{\Gamma_1}{4\pi}\log\left(r^2+\rho_1^2-2r\rho_1\cos(\theta-\alpha_1)\right)-\frac{\Gamma_2}{4\pi}\log\left(r^2+\rho_2^2-2r\rho_2\cos(\theta-\alpha_2)\right)\\ &\quad+\frac{\Gamma_1}{4\pi}\log\left(r^2\rho_1^2+a^4-2r\rho_1a^2\cos(\theta-\alpha_1)\right)+\frac{\Gamma_2}{4\pi}\log\left(r^2\rho_2^2+a^4-2r\rho_2a^2\cos(\theta-\alpha_2)\right)\\ &\quad-\frac{(\Gamma_1+\Gamma_2)}{2\pi}\log(r). \end{aligned} \tag{2}$$

The velocity of vortex 1 can then be found by calculating the induced velocity at $z = z_1 = \rho_1 e^{\mathrm{i}\alpha_1}$ due to the other physical vortex and the image vortices. Thus the governing ordinary differential equations (ODEs) for the motion of vortex 1 are

$$\begin{aligned}\frac{\mathrm{d}\rho_1}{\mathrm{d}t} = \frac{1}{r}\left.\frac{\partial\psi}{\partial\theta}\right|_{z=z_1} &= -\frac{\Gamma_2}{2\pi}\frac{\rho_2\sin(\alpha_1-\alpha_2)}{[\rho_1^2+\rho_2^2-2\rho_1\rho_2\cos(\alpha_1-\alpha_2)]}\\ &\quad+\frac{\Gamma_2}{2\pi}\frac{a^2\rho_2\sin(\alpha_1-\alpha_2)}{[\rho_1^2\rho_2^2+a^4-2\rho_1\rho_2a^2\cos(\alpha_1-\alpha_2)]}, \end{aligned} \tag{3}$$

$$\begin{aligned}\rho_1\frac{\mathrm{d}\alpha_1}{\mathrm{d}t} = -\left.\frac{\partial\psi}{\partial r}\right|_{z=z_1} &= \frac{\Gamma_2}{2\pi}\frac{\rho_1-\rho_2\cos(\alpha_1-\alpha_2)}{[\rho_1^2+\rho_2^2-2\rho_1\rho_2\cos(\alpha_1-\alpha_2)]}\\ &\quad-\frac{\Gamma_2}{2\pi}\frac{\rho_2(\rho_1\rho_2-a^2\cos(\alpha_1-\alpha_2))}{[\rho_1^2\rho_2^2+a^4-2\rho_1\rho_2a^2\cos(\alpha_1-\alpha_2)]}\\ &\quad-\frac{\Gamma_1}{2\pi}\frac{\rho_1}{[\rho_1^2-a^2]}+\frac{(\Gamma_1+\Gamma_2)}{2\pi\rho_1}. \end{aligned} \tag{4}$$

Similarly the governing equations for vortex 2 can be shown to be

$$\begin{aligned}\frac{\mathrm{d}\rho_2}{\mathrm{d}t} &= -\frac{\Gamma_1}{2\pi}\frac{\rho_1\sin(\alpha_2-\alpha_1)}{[\rho_1^2+\rho_2^2-2\rho_1\rho_2\cos(\alpha_1-\alpha_2)]}\\ &\quad+\frac{\Gamma_1}{2\pi}\frac{a^2\rho_1\sin(\alpha_2-\alpha_1)}{[\rho_1^2\rho_2^2+a^4-2\rho_1\rho_2a^2\cos(\alpha_1-\alpha_2)]}, \end{aligned} \tag{5}$$

$$\begin{aligned}\rho_2\frac{\mathrm{d}\alpha_2}{\mathrm{d}t} &= \frac{\Gamma_1}{2\pi}\frac{\rho_2-\rho_1\cos(\alpha_2-\alpha_1)}{[\rho_1^2+\rho_2^2-2\rho_1\rho_2\cos(\alpha_1-\alpha_2)]}\\ &\quad-\frac{\Gamma_1}{2\pi}\frac{\rho_1(\rho_1\rho_2-a^2\cos(\alpha_1-\alpha_2))}{[\rho_1^2\rho_2^2+a^4-2\rho_1\rho_2a^2\cos(\alpha_1-\alpha_2)]}\\ &\quad-\frac{\Gamma_2}{2\pi}\frac{\rho_2}{[\rho_2^2-a^2]}+\frac{(\Gamma_1+\Gamma_2)}{2\pi\rho_2}. \end{aligned} \tag{6}$$

In the limit as $a\to\infty$, with $\alpha_j = x_j/a$ and $\rho_j = a+y_j$ for $j=1,2$, equations (3)-(6) reduce to the equivalent planar wall equations, e.g. (14)-(17) in [19].

The above system is Hamiltonian with respect to the conjugate variables

$$(q_j,p_j) = (\Gamma_j\rho_j,\rho_j\alpha_j), \quad \text{for} \quad j=1,2,$$

with the Hamiltonian given by

$$\begin{aligned}\mathcal{H}(\rho_1,\alpha_1,\rho_2,\alpha_2;a) = \frac{1}{4\pi}\log\Bigg[&\rho_1^{-2\Gamma_1(\Gamma_1+\Gamma_2)}\rho_2^{-2\Gamma_2(\Gamma_1+\Gamma_2)}(\rho_1^2-a^2)^{\Gamma_1^2}(\rho_2^2-a^2)^{\Gamma_2^2}\\ &\left[\frac{\rho_1^2\rho_2^2+a^4-2\rho_1\rho_2a^2\cos(\alpha_1-\alpha_2)}{\rho_1^2+\rho_2^2-2\rho_1\rho_2\cos(\alpha_1-\alpha_2)}\right]^{\Gamma_1\Gamma_2}\Bigg]. \end{aligned} \tag{7}$$

Note, that here Hamilton's equations

$$(\dot{q}_j, \dot{p}_j) = \left(\frac{\partial \mathcal{H}}{\partial p_j}, -\frac{\partial \mathcal{H}}{\partial q_j} \right),$$

become

$$(\Gamma_j \dot{\rho}_j, \dot{\overline{\rho_j \alpha_j}}) = \left(\frac{1}{\rho_j} \frac{\partial \mathcal{H}}{\partial \alpha_j}, -\Gamma_j^{-1} \frac{\partial \mathcal{H}}{\partial \rho_j} + \frac{\alpha_j}{\Gamma_j \rho_j} \frac{\partial \mathcal{H}}{\partial \alpha_j} \right).$$

From (3) and (5) we observe that the combination $\Gamma_1 \rho_1 *(3) + \Gamma_2 \rho_2 *(5)$ leads to

$$\Gamma_1 \rho_1 \frac{\mathrm{d}\rho_1}{\mathrm{d}t} + \Gamma_2 \rho_2 \frac{\mathrm{d}\rho_2}{\mathrm{d}t} = 0,$$

and hence by integrating with respect to t, we can define the conserved quantity

$$\rho_0^2 = \frac{\Gamma_1 \rho_1^2 + \Gamma_2 \rho_2^2}{\Gamma_1 + \Gamma_2}, \tag{8}$$

which is the absolute value of the momentum of the flow, scaled by the total circulation [28]. This definition is valid as we have excluded the case when $\Gamma_1 + \Gamma_2 = 0$. In this case the conserved quantity (8) becomes $\rho_1^2 - \rho_2^2$, and because this is conserved it cannot change sign during the motion of the vortices, and hence the vortices cannot change their radial ordering with respect to the cylinder surface. Thus no leapfrogging is observed, and the vortices either just move around the cylinder in near circular orbits, or propagate away from the cylinder as a vortex pair.

Using definition (8), we define the two dimensionless relative coordinates

$$R(t) = \frac{\rho_2^2 - \rho_1^2}{\rho_0^2} \quad \text{and} \quad A(t) = \alpha_2 - \alpha_1, \tag{9}$$

such that

$$\rho_1 = \rho_0 \left[1 - g_2 R\right]^{1/2} \quad \text{and} \quad \rho_2 = \rho_0 \left[1 + g_1 R\right]^{1/2}, \tag{10}$$

where

$$g_1 = \frac{\Gamma_1}{\Gamma_1 + \Gamma_2} \quad \text{and} \quad g_2 = \frac{\Gamma_2}{\Gamma_1 + \Gamma_2}.$$

The Hamiltonian of the system (7) is the kinetic energy of the system, which is conserved, thus we can set (7) equal to a constant such that

$$\frac{1}{4\pi} \log \Bigg[\rho_1^{-2\Gamma_1(\Gamma_1+\Gamma_2)} \rho_2^{-2\Gamma_2(\Gamma_1+\Gamma_2)} (\rho_1^2 - a^2)^{\Gamma_1^2} (\rho_2^2 - a^2)^{\Gamma_2^2} \left[\frac{\rho_1^2 \rho_2^2 + a^4 - 2\rho_1 \rho_2 a^2 \cos(\alpha_1 - \alpha_2)}{\rho_1^2 + \rho_2^2 - 2\rho_1 \rho_2 \cos(\alpha_1 - \alpha_2)} \right]^{\Gamma_1 \Gamma_2} \Bigg] = \frac{\Gamma_1 \Gamma_2}{4\pi} \log \frac{C}{\rho_0^2},$$

where C is an unspecified constant. Writing the above expression in terms of (9) and (10), it can be expressed as

$$[1 - g_2 R]^{-1/g_2} [1 + g_1 R]^{-1/g_1} [1 - g_2 R - d^2]^{g_1/g_2} [1 + g_1 R - d^2]^{g_2/g_1} \left[\frac{[1 - g_2 R][1 + g_1 R] + d^4 - 2d^2 [1 - g_2 R]^{1/2} [1 + g_1 R]^{1/2} \cos(A)}{2 + (g_1 - g_2) R - 2[1 - g_2 R]^{1/2} [1 + g_1 R]^{1/2} \cos(A)} \right] = C, \tag{11}$$

where $d = a/\rho_0$ is the non-dimensional cylinder radius. Equation (11) describes solution trajectories in the (A, R)-phase plane for different values of C. For the case of two vortices next to an impermeable barrier orientated with the $x-$axis, equivalent to the problem studied by [19], it was found that the phase-plane includes both closed and open trajectories. The closed trajectories signified periodic solutions where the vortices leapfrog past one another, while the open trajectories signified solutions where the vortices either never pass one another, or only pass each other once, i.e. non-leapfrogging motions. The two different solution types are separated by a separatrix, which corresponds to a critical value of the constant C, namely C_{crit}, which leads to a condition for leapfrogging vortices. By leapfrogging, we are referring to the scenario where both vortices travel in the same direction around the cylinder, the trailing vortex is pushed closer to the cylinder by the leading vortex, which in turn forces the leading vortex away from the cylinder. This effect causes the leading vortex to slow down and the trailing vortex to speed up, which allows the trailing vortex to overtake the leading vortex, passing between the vortex and the cylinder. This process then continues to repeat periodically. The criteria for this leapfrogging motion is derived in the next section.

2.2 Criteria for leapfrogging vortices

In [19] the separatrix in the solution phase-plane occurs at the point of maximum separation of the vortices for the case when both vortices have strengths of the same sign. In the current work we also consider this case, as well as the case when the vortices have strengths of opposite sign. Investigating the solution trajectories in the (A, R)-plane by directly integrating (3)-(6), we find the cases for $\mu = \Gamma_2/\Gamma_1 = g_2/g_1 > 0$ and $\mu < 0$ have different structures, similar to what has been observed for vortex rings [18]. We consider these cases here.

For $0 < \mu \leq 1$ the separatrix occurs at the maximum azimuthal separation of the vortices, namely when $A = \pi$, and thus we can define the function

$$F^+(R; d, g_1, g_2) := [1 - g_2R]^{-1/g_2}[1 + g_1R]^{-1/g_1}(1 - g_2R - d^2)^{g_1/g_2}(1 + g_1R - d^2)^{g_2/g_1} \left(\frac{[1 - g_2R][1 + g_1R] + d^4 + 2d^2[1 - g_2R]^{1/2}[1 + g_1R]^{1/2}}{2 + (g_1 - g_2)R + 2[1 - g_2R]^{1/2}[1 + g_1R]^{1/2}} \right). \quad (12)$$

The function $F^+(R; d, g_1, g_2)$ is essentially the LHS of (11) and thus where $F^+(R) = C$ gives real values, this corresponds to a phase plane trajectory in the (A, R)-plane. Note, however that for our purposes the function $F^+(R; d, g_1, g_2)$ is not valid for all values of R, and in fact for the vortices to lie outside the cylinder ($\rho_{1,2} > a$) we require from (10) that

$$\frac{d^2 - 1}{g_1} < R < \frac{1 - d^2}{g_2}. \quad (13)$$

Figures 2(a) and 2(b) plot $F^+(R)$ for $\mu = 0.15,\ 0.5,\ 0.8$ for $d = 0.6$ and $d = 0.2$ respectively. These results show that the function $F^+(R)$ has a maximum value at $R = R_{\text{max}}$ in the range (13), where $F^+(R_{\text{max}}) = C_{\text{crit}}$. Unlike for the planar wall case, there is no closed form for the value of C_{crit} and hence this value needs to be solved for numerically using Newton iterations. A contour plot of $C_{\text{crit}}(\mu, d)$ is given in figure 2(c), and shows that for a fixed $d \lesssim 0.5$, increasing μ from $\mu \approx 0$ leads to C_{crit} increasing to some maximum value before decreasing again towards $\mu = 1$. For fixed $d \gtrsim 0.5$ increasing μ

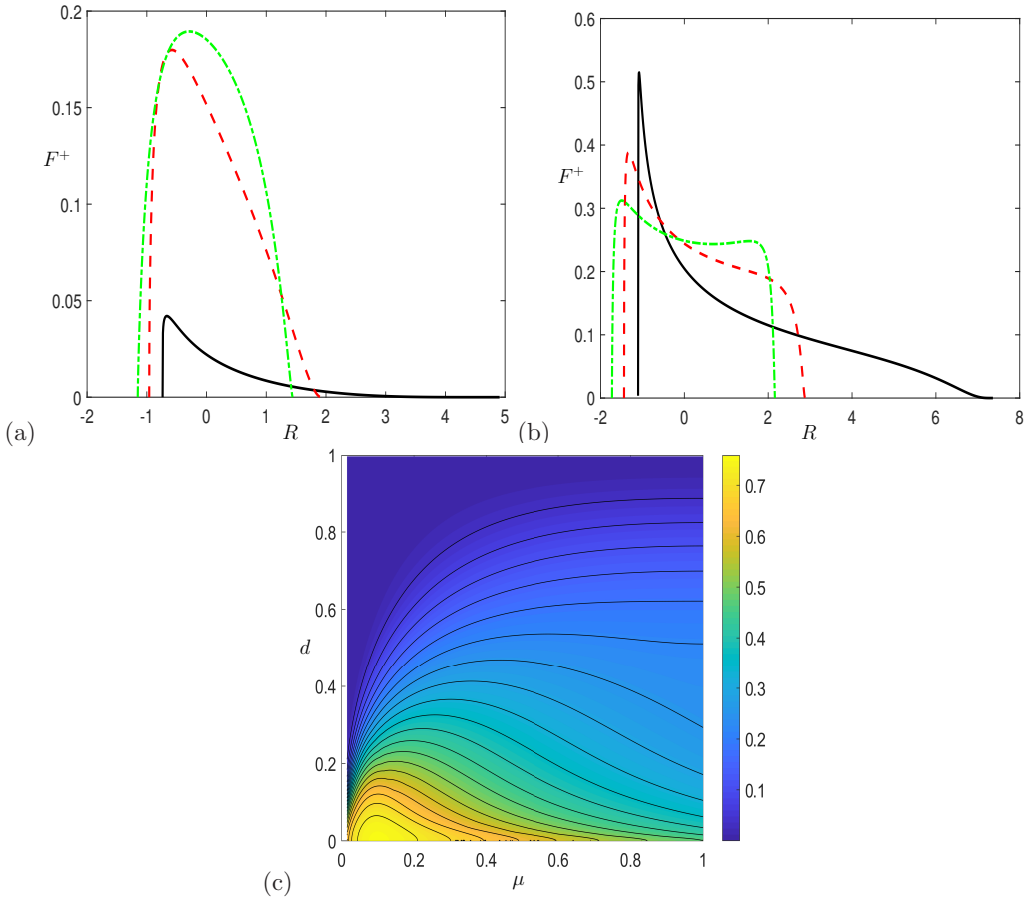

Figure 2: (colour online) Plot of $F^+(R)$ for $\mu = 0.15$ (solid curve), 0.5 (dashed curve), 0.8 (dot-dashed curve) for (a) $d = 0.6$ and (b) $d = 0.2$. Panel (c) plots $C_{\rm crit}(\mu, d)$.

just increases the value of $C_{\rm crit}$ up to its $\mu = 1$ value, at a relatively slow rate. Note, that $C_{\rm crit}(\mu, d)$ for $\mu \geq 1$ are just $C_{\rm crit}(\mu^{-1}, d)$ where $0 < \mu \leq 1$.

Note, in figure 2(b) the dot-dashed curve, $\mu = 0.8$, has two distinct maximum values in the range (13), with the second maximum having $C^{(2)}_{\rm max} < C_{\rm crit}$. Thus in this case the (A, R)-phase plane will have two separatrices along the line $A = \pi$. However, we will show in 3 that it is only for values of $C > C_{\rm crit}$ that we have leapfrogging motions, while for $C^{(2)}_{\rm max} < C < C_{\rm crit}$ we have another non-leapfrogging solution.

For the case $-1 < \mu < 0$, a numerical investigation of the (A, R)-plane now shows the separatrix occurs at $A = 0$ and thus we define

$$F^-(R; d, g_1, g_2) := [1 - g_2 R]^{-1/g_2}[1 + g_1 R]^{-1/g_1}(1 - g_2 R - d^2)^{g_1/g_2}(1 + g_1 R - d^2)^{g_2/g_1} \left(\frac{[1 - g_2 R][1 + g_1 R] + d^4 - 2d^2[1 - g_2 R]^{1/2}[1 + g_1 R]^{1/2}}{2 + (g_1 - g_2)R - 2[1 - g_2 R]^{1/2}[1 + g_1 R]^{1/2}} \right), \quad (14)$$

which by requiring $\rho_{1,2} > 0$ in (10) with $g_2 < 0$, leads to the validity condition

$$\frac{d^2 - 1}{g_1} < R.$$

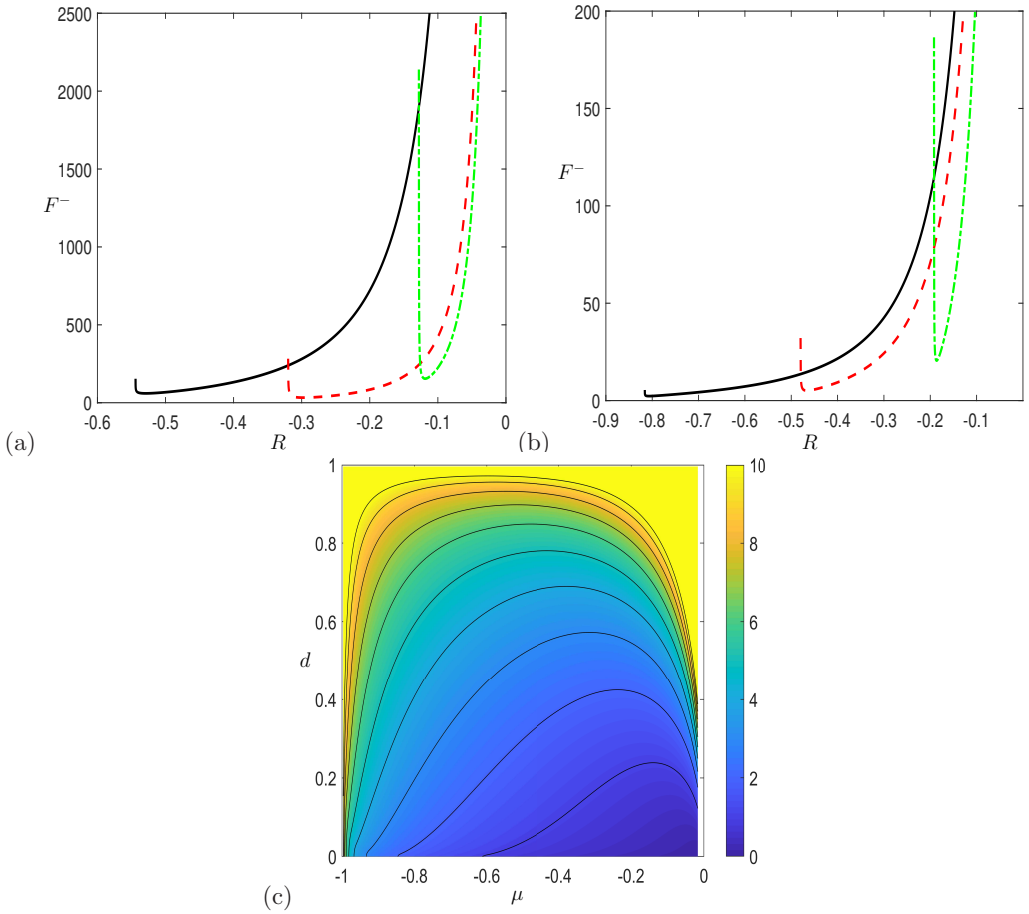

Figure 3: (colour online) Plot of $F^-(R)$ for $\mu = -0.15$ (solid curve), -0.5 (dashed curve), -0.8 (dot-dashed curve) for (a) $d = 0.6$ and (b) $d = 0.2$. Panel (c) plots $\log(C_{\rm crit}(\mu, d))$, and note the scale change in $C_{\rm crit}$ values compared to figure 2.

In figures 3(a) and 3(b) we plot $F^-(R)$ for $\mu = -0.15, \ -0.5, \ -0.8$ for $d = 0.6$ and $d = 0.2$ respectively. In this case as $\mu < 0$, $F^- \to \infty$ as $R \to (d^2 - 1)/g_1$ and $R \to 0$. Beyond $R = 0$, $F^- \to 0$ as $R \to \infty$ (not shown). The key thing in this case is that F^- has a minimum at $R = R_{\rm min} \in ((d^2 - 1)/g_1, 0)$. Thus there are no real values of C satisfying $C < C_{\rm crit} = F^-(R_{\rm min})$, which defines the critical value. We again expect to find periodic leapfrogging motions for $C > C_{\rm crit}$, except for values of $R < R_{\rm min}$ where there is no leapfogging. In figure 3(c) we plot $\log(C_{\rm crit})$, as the values of $C_{\rm crit}$ can become very large in this case, and also we find that $C_{\rm crit}$ for a fixed d has a minimum value for $\mu \in (-1, 0)$.

When $C = C_{\rm crit}$ in (11) this equation can be considered as giving the maximal initial spacing of the vortices, in the azimuthal direction, $A_{\rm max}$, for a given initial radial displacement $R(0)$ in the form

$$\cos(A_{\rm max}) = \frac{\gamma(g_1, g_2, d, R)\left([1 - g_2R][1 + g_1R] + d^4\right) - C_{\rm crit}\left(2 + (g_1 - g_2)R\right)}{2[1 - g_2R]^{1/2}[1 + g_1R]^{1/2}\left(\gamma(g_1, g_2, d, R)d^2 - C_{\rm crit}\right)}, \qquad (15)$$

where

$$\gamma(g_1, g_2, d, R) = [1 - g_2R]^{-1/g_2}[1 + g_1R]^{-1/g_1}[1 - g_2R - d^2]^{g_1/g_2}[1 + g_1R - d^2]^{g_2/g_1}.$$

Thus we have leapfrogging when the initial azimuthal separation satisfies $-A_{\max} < A(0) < A_{\max}$. Note that equally we could have considered (11) with $C = C_{\text{crit}}$ as giving the maximal radial spacing for a given initial azimuthal spacing. Contour plots of $A_{\max}(R, d)/\pi$ are given in figure 4. These figures show that for fixed (R, d) values, the value of $A_{\max}$

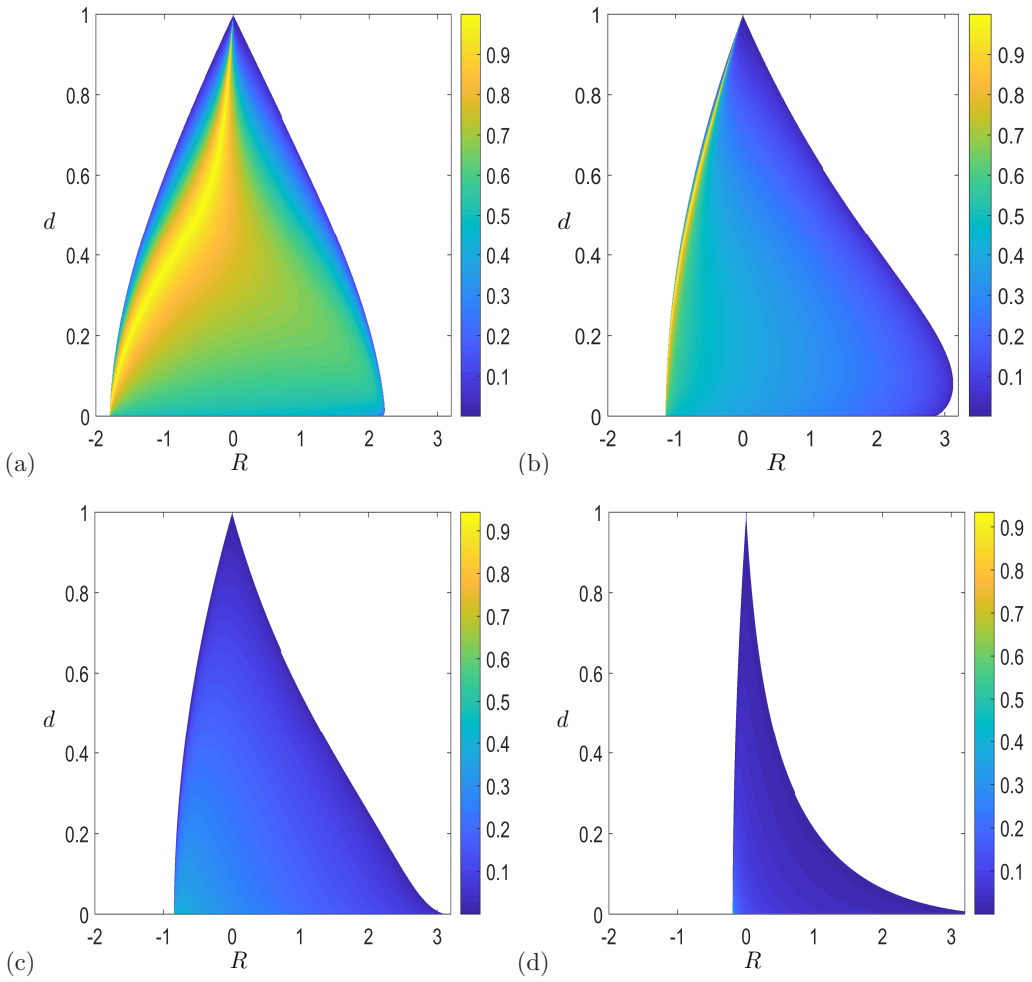

Figure 4: (colour online) Contour plots of $A_{\max}(R, d)/\pi$ for (a) $\mu = 0.8$, (b) $\mu = 0.15$, (c) $\mu = -0.15$ and (d) $\mu = -0.8$. Note, in the white regions of these figures no leapfrogging is possible.

typically reduces as μ reduces, i.e. as the strength of the two vortices diverge. For $0 < \mu \leq 1$ in panels (a) and (b), the maximum value of $A_{\max} = \pi$ (because the separatrix lies at $A = \pi$) occurs when $R < 0$, i.e. when the stronger vortex (vortex 1) is furthest from the cylinder. For $-1 < \mu < 0$ the maximum value of $A_{\max}$ is not π and figures 4(c) and 4(d) show the value of $A_{\max}$ is generally smaller, showing that leapfrogging is only possible if the vortices are initially close together.

In 3 we demonstrate the existence of this leapfrogging region by examining the trajectories of the two vortices with initial separations either side of this critical $A_{\max}$ value.

3 Vortex Trajectory Results

Here we demonstrate the leapfrogging phenomena of two line vortices external to a circular cylinder by examining their trajectories for distinct values of $\mu = g_2/g_1$ and d. We begin by considering contour plots of the $(A/\pi, R)$-phase plane in figure 5. Here we consider

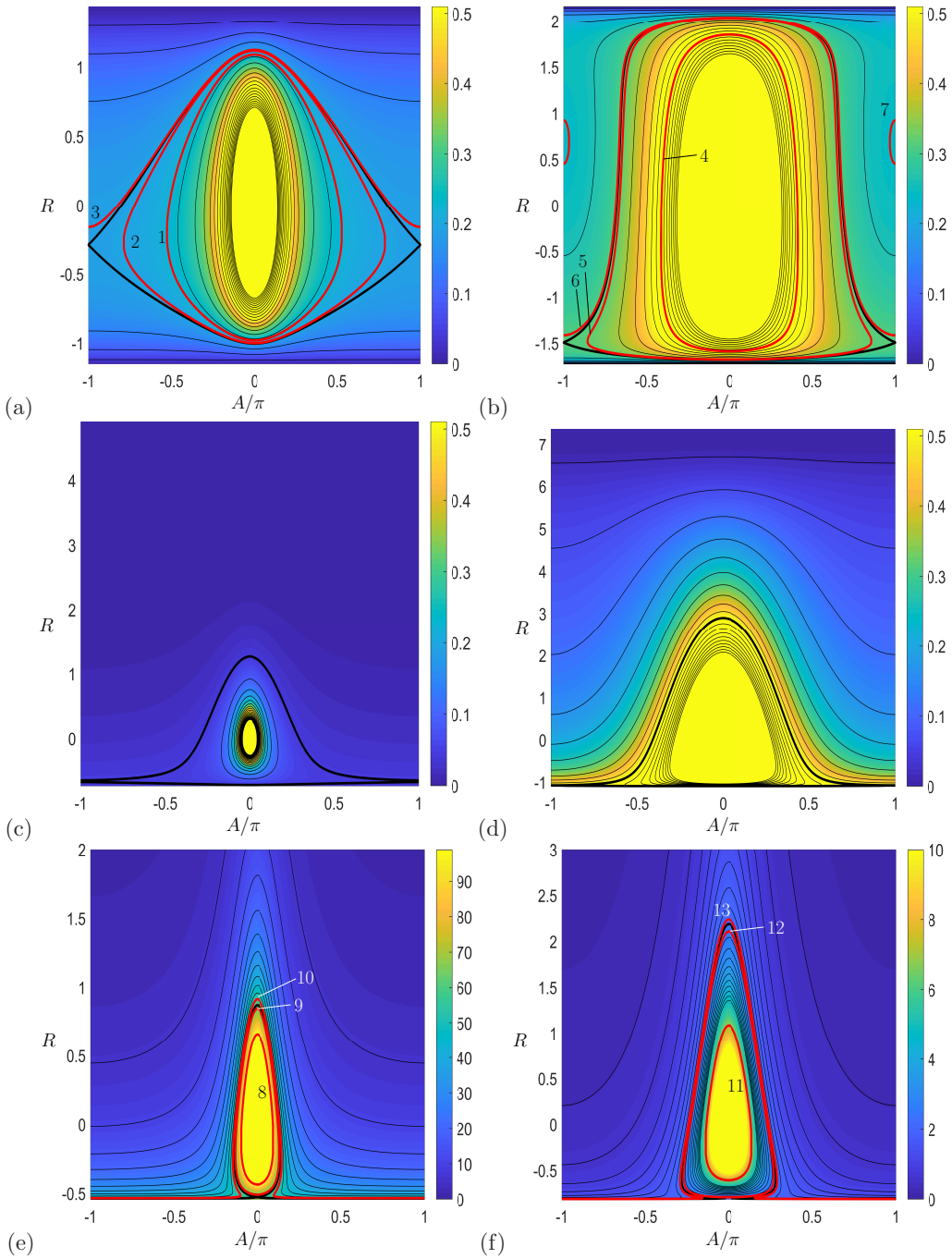

Figure 5: (colour online) Contour plot of $C(A/\pi, R)$ for (a) $(\mu, d) = (0.8, 0.6)$, (b) $(0.8, 0.2)$, (c) $(0.15, 0.6)$, (d) $(0.15, 0.2)$, (e) $(-0.15, 0.6)$ and (f) $(-0.15, 0.2)$. The thick black contour signifies the value of C_{crit} in each case, and in panels (a), (b), (e) and (f) the thick numbered contours represent those results presented in figures 6 to 9.

the six combinations of results with $\mu = 0.8$, 0.15 and -0.15 with $d = 0.6$ and 0.2. The results indicate that smaller cylinders typically have a larger region in the phase-plane where leapfrogging occurs, and thus the phase-planes for $d = 0.6$ are narrower in the A/π direction for a given value of R (except around the separatrix). Leapfrogging occurs for contours inside the C_{crit} contour (thick black contour), i.e. $C > C_{\text{crit}}$, and these contours are traversed clockwise for $\mu > 0$ (with $\Gamma_{1,2} > 0$) and for $\mu < 0$ (with $\Gamma_1 > 0$). Close to $(0, 0)$ the period of the leapfrogging motion tends to zero, while at the separatrix the period tends to infinity.

The thicker contours (red online) in figures 5(a), 5(b), 5(e) and 5(f) numbered 1-13 denote cases examined below by numerically integrating the governing ODEs (3)-(6). The ODEs are integrated forward in time using a 4th order Runge-Kutta scheme from an initial condition which lies on one of the numbered contours with a time-step $\Delta t = 10^{-3}$. Note, the timescale of the simulations is governed by the quantity Γ_1/a^2 in this work. This is equivalent to non-dimensionalizing equations (3)-(6) using the non-dimensional time $\tau = \frac{\Gamma_1}{a^2}t$. In the absence of the second vortex, vortex 1 should complete an orbit of the cylinder every $\frac{4\pi^2 a^2}{\Gamma_1 \rho_1^2(\rho_1^2 - a^2)}$ seconds. The respective parameters and initial conditions are given in table 1, while in all the cases presented the initial radial separation of the vortices is taken as $R(0) = 0.5$.

Contour number	Trajectory figures	Γ_2	d	a	$\rho_2(0)$	$\alpha_2(0)$	$A_{\max}$	C	C_{crit}
1	6(a,b)	0.8	0.6	0.6803	1.2817	0.4π	0.5246π	0.2224	0.1895
2	6(c,d)	0.8	0.6	0.6803	1.2817	0.5π	0.5246π	0.1941	0.1895
3	6(e,f)	0.8	0.6	0.6803	1.2817	0.53π	0.5246π	0.1885	0.1895
4	8(a,b)	0.8	0.2	0.2268	1.2817	0.4π	0.6650π	0.6193	0.3123
5	8(c,d)	0.8	0.2	0.2268	1.2817	0.65π	0.6650π	0.3200	0.3123
6	8(e,f)	0.8	0.2	0.2268	1.2817	0.67π	0.6650π	0.3098	0.3123
7	8(g,h)	0.8	0.2	0.2268	1.2817	0.98π	0.6650π	0.2440	0.3123
8	—	-0.15	0.6	0.5752	1.2081	0.05π	0.0838π	101.6328	59.9648
9	—	-0.15	0.6	0.5752	1.2081	0.08π	0.0838π	63.4966	59.9648
10	—	-0.15	0.6	0.5752	1.2081	0.09π	0.0838π	54.8160	59.9648
11	—	-0.15	0.2	0.1917	1.2081	0.1π	0.1962π	6.9117	2.3084
12	—	-0.15	0.2	0.1917	1.2081	0.19π	0.1962π	2.4410	2.3084
13	—	-0.15	0.2	0.1917	1.2081	0.20π	0.1962π	2.2325	2.3084

Table 1: Parameter values and initial conditions used when integrating the ODEs (3)-(6) for the trajectories in figures 6-9. In each case $R(0) = 0.5$, $\rho_1(0) = 1$, $\alpha_1(0) = 0$ and $\Gamma_1 = 1$.

In figure 6 we plot trajectories of the vortices in the (r, θ)- and (x, y)-planes for the case $d = 0.6$ and $\mu = 0.8$, which has $A_{\max} = 0.5246\pi$ with $R(0) = 0.5$. In figures 6(a) and 6(b) we consider the case $A(0) = 0.4\pi < A_{\max}$ and hence we expect, and observe, leapfrogging of the vortices, as seen in panel (a). Note, we choose to plot the absolute angles $\alpha_1(t)$ and $\alpha_2(t)$, not their principal values, as this allows for less congested figures in which the leapfrogging motion is clearer. In panel (a) we observe that both vortices are travelling clockwise around the cylinder and we see that the vortices regularly cross

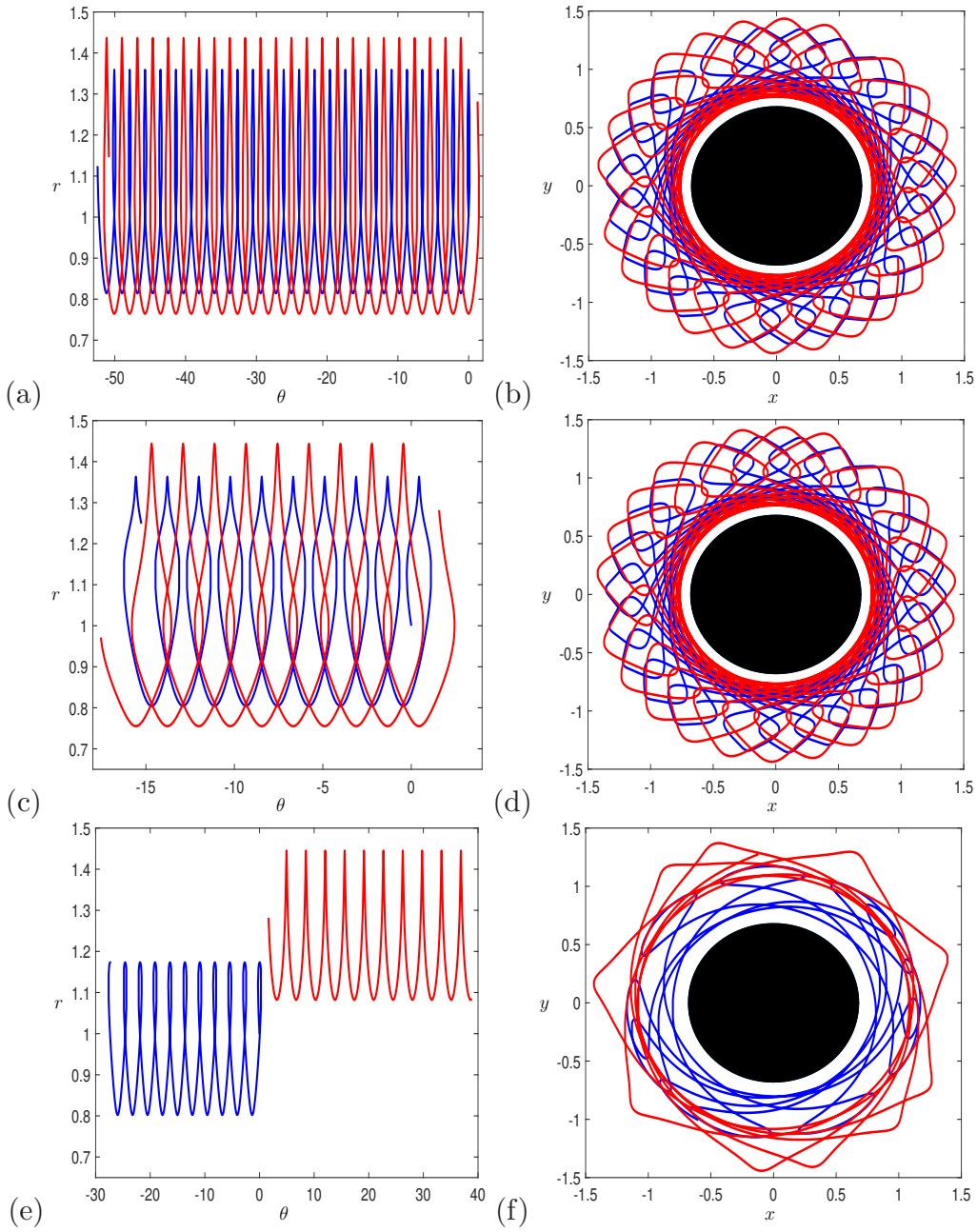

Figure 6: (colour online) Plot of (a,c,e) $(\theta, r)-$plane and (b,d,f) $(x, y)-$plane for $\mu = 0.8$, $d = 0.6$, and the inital vortex separation conditions $R(0) = 0.5$ and (a,b) $A(0) = 0.4\pi$, (c,d) $A(0) = 0.5\pi$ and (e,f) $A(0) = 0.53\pi$. These 3 cases correspond to the paths numbered 1-3 respectively in the phase-plane figure 5(a). In each panel the darker line (blue) represents vortex 1 while the lighter line (red) represents vortex 2.

paths, with the outer vortex forced toward the cylinder in order to speed up and overtake the inner vortex. In figure 6(b) we see the vortex trajectories in the physical (x, y)-plane which shows that when the vortices are forced outward to larger radii they reverse their direction for a short period of time creating lobe like structures. In figures 6(c) and 6(d) $A(0) = 0.5\pi$ which is still less than $A_{\max}$, and so we again have leapfrogging of the

vortices but with a larger period of the motion, and in figure 6(c) the direction reversal of the vortices is more obvious. In figures 6(e) and 6(f) we consider an initial separation of the vortices with $A(0) = 0.53\pi > A_{\max}$, and hence we do not expect to see leapfrogging in this case, and in fact the vortices travel in opposite directions around the cylinder (vortex 1, clockwise and vortex 2, counter-clockwise). The vortices do still interact with one another when their principal angles become comparable, but they do not regularly switch positions with each another. Here in figure 6(f) we do still see some direction reversal for vortex 1, but not for vortex 2 in this case.

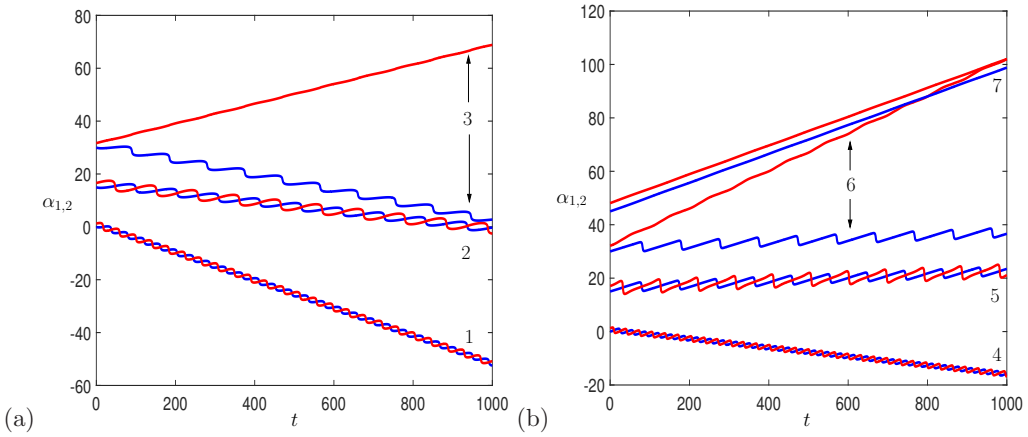

Figure 7: Plot of $\alpha_j(t)$ for vortex $j = 1$ (dark curve, blue), 2 (light curve, red) for $\mu = 0.8$ and (a) $d = 0.6$ and (b) $d = 0.2$. In each panel the numbering of the results corresponds to that in figures 5(a) and 5(b) respectively, and the results are separated by the constant 20 for clarity.

The leapfrogging of the vortices is not always clear in the physical-plane as the trajectories soon clutter the figure, but it is more readily visible by plotting the absolute angles of the vortices, $\alpha_{1,2}$ as a function of time. Figure 7(a) plots these quantities for cases 1-3 in figure 6. For cases 1 and 2, leapfrogging can be observed, while for case 3, there is no leapfrogging as the vortices are travelling in opposite directions, as per figure 6(e).

In figure 8 we consider vortex trajectories as in figure 6, but in this case we consider a smaller cylinder, with $d = 0.2$, which with $R(0) = 0.5$ gives $A_{\max} = 0.6650\pi$. The results in figures 8(a) and 8(c), $A = 0.4\pi$ and $A = 0.65\pi$ respectively, both exhibit leapfrogging, as predicted, with the panel (c) results again having a much larger period than in panel (a). Compared to the larger cylinder case in figure 6, here we find the vortices undergo a more sustained region of reversed motion (in the counter-clockwise direction). In figure 8(e) $A(0) = 0.67\pi > A_{\max}$ and thus there is no leapfrogging, but clearly there is still a large amount of interaction between the two vortices, more so than in figure 6, as the range of radial values covered by the vortices is larger here. Unlike for the case in figure 6(e), here both vortices travel counter-clockwise around the cylinder, but with vortex 2 (light curve, red) travelling significantly faster. In general, as A is increased towards $A_{\max}$ (or decreased towards $-A_{\max}$) for a given value of $R(0)$, the speed of the vortices reduces and the period of the motion increases. Then for $0 > A(0) - A_{\max} \gg -1$ the vortices change direction but keep on leapfrogging one another as for result 5 in figure 7(b), which plots the time evolution of $\alpha_{1,2}(t)$ for the cases in figure 8. As $A(0)$ passes

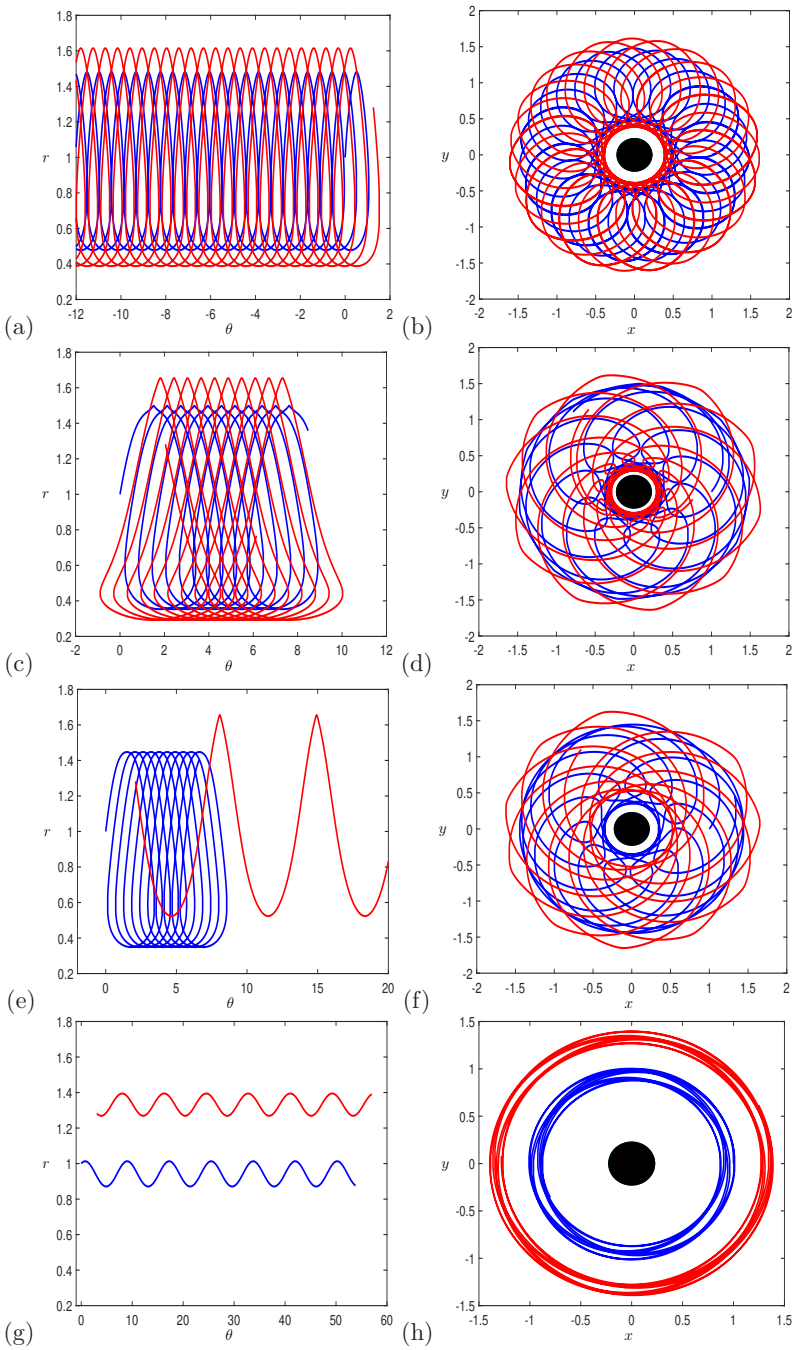

Figure 8: (colour online) Plot of (a,c,e,g) $(\theta, r)-$plane and (b,d,f,h) $(x, y)-$plane for $\mu = 0.8$, $d = 0.2$, and the inital vortex separation conditions $R(0) = 0.5$ and (a,b) $A(0) = 0.4\pi$, (c,d) $A(0) = 0.65\pi$, (e,f) $A(0) = 0.67\pi$ and (g,h) $A(0) = 0.98\pi$. These 4 cases correspond to the paths numbered 4-7 respectively in the phase-plane in figure 5(b). In each panel the darker line (blue) represents vortex 1 while the lighter line (red) represents vortex 2.

over the separatrix so that now $1 \gg A(0) - A_{\max} > 0$ then the vortices no longer leapfrog one another, but both remain travelling in the counter-clockwise direction, see result 6 in figure 7(b). As A is increased further, then the direction of vortex 1 changes such that

the vortices now travel in opposite directions, see result 3 from figure 7(a).

If however, the (A, R)-plane also has closed contours centred on $A = \pi$, as is the case for result 7 in figure 5(b), then there is an additional form of solution which is possible, given in figures 8(g) and 8(h). Here the initial condition places the two vortices almost on opposite sides of the cylinder. In this case the vortices remain approximately π out of phase with one another and so their interaction is much weaker. In the physical-plane in panel (h) this shows two vortices completing near circular orbits of the cylinder, with each perturbed slightly by the other vortex. Here both vortices are travelling counter-clockwise around the cylinder.

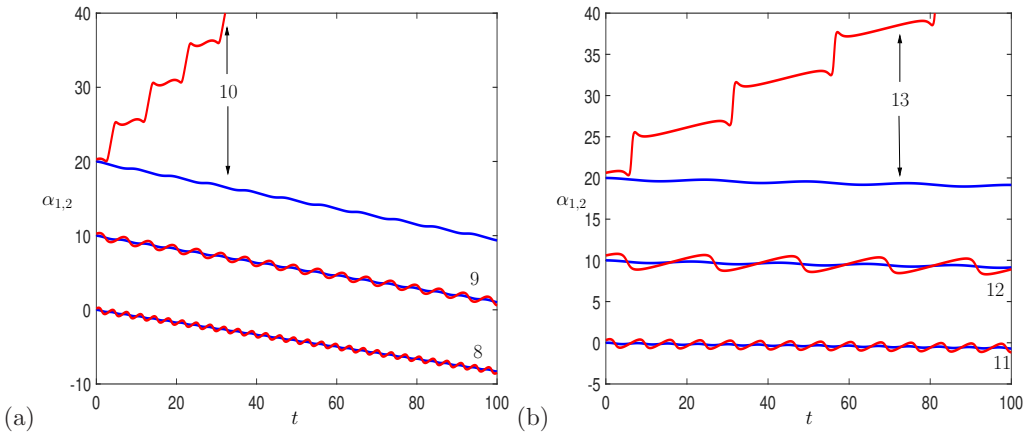

Figure 9: Plot of $\alpha_j(t)$ for vortex $j = 1$ (dark curve, blue), 2 (light curve, red) for $\mu = -0.15$ and (a) $d = 0.6$ and (b) $d = 0.2$. In each panel the numbering of the results corresponds to that in figures 5(e) and 5(f) respectively, and the results are separated by the constant 10 for clarity.

Finally we consider cases for $\mu < 0$ in figure 9. As the most illuminating plots for identifying leapfrogging are the time evolution plots of $\alpha_{1,2}(t)$, we consider only these for cases 8-13 from figures 5(e) and 5(f). The results agree completely with those already documented in figure 7 and thus proves that leapfrogging around a circular cylinder can also occur with vortices with strengths of opposite sign. A result already known for vortex rings [29].

4 Conclusions and Discussion

In this article a criteria indicating when two interacting point vortices of differing strengths, in the vicinity of an impermeable circular cylinder, undergo periodic leapfrogging is derived. The criteria is a function of the vortex strength ratio, $\mu = \Gamma_1/\Gamma_2$, and the radius of the cylinder, a. This criteria is determined as a critical constant C_{crit} such that we get leapfrogging for $C > C_{\text{crit}}$ where C is given by (11). Unlike in the infinite, straight barrier case studied by [19], the vortices don't separate completely for $C < C_{\text{crit}}$ due to the periodic geometry, and in this case we find weak, non-leapfrogging interactions of the two vortices.

In the numerical results presented, we chose to consider a fixed radial spacing of the vortices initially, which leads the condition $C > C_{\text{crit}}$ being considered as a condition on

the initial azimuthal spacing $A(0)$ being less than some critical value $A_{\max}$ for leapfrogging to occur. For $\Gamma_1 \geq \Gamma_2 > 0$ the leapfrogging motion occurs with both vortices moving clockwise around the cylinder. For a fixed $A(0)$ value, as the critical value of $A_{\max}$ is approached from below, the velocity of the vortices slow until they begin to leapfrog in the counter-clockwise direction. Beyond the critical azimuthal separation $A_{\max}$ we find that the speed of the weaker vortex, vortex 2, increases greatly and hence moves too fast to leapfrog with vortex 1. Increasing the radial separation further causes the vortices to travel in opposite directions around the cylinder, only weakly interacting with each other when their azimuthal coordinates are comparable. For small values of $\Gamma_1/\Gamma_2 > 0$ and small cylinders, a second separatrix forms in the (A, R)-plane, and when the vortex pair have initial conditions which puts them in this part of the phase space, the vortices again travel in the same direction, counter-clockwise this time, but their azimuthal separation oscillates around a value of π. Hence there is very little interaction in this case. We also identify leapfrogging for vortices with strengths of different sign ($\Gamma_1/\Gamma_2 < 0$ and $\Gamma_1 + \Gamma_2 \neq 0$). In this case the values of $A_{\max}$ for a given radial separation are typically much smaller than for $\Gamma_1/\Gamma_2 > 0$, meaning the vortices need to initially be closer together to observe leapfrogging.

The theory presented here can be extended to examine the motion of two line vortices exterior to other closed barriers by using conformal mappings. It can be shown by following the work of [30] and [28] that given a conformal mapping $z = G(Z)$ between the complex z- and Z-planes, that the Hamiltonians in both planes for two line vortices are related via

$$\mathcal{H}_z(z_1, z_2) = \mathcal{H}_Z(Z_1, Z_2) + \frac{1}{4\pi}\sum_{j=1}^{2}\Gamma_j^2 \log|G'(Z_j)| + \sum_{j=1}^{2}\Gamma_j \mathrm{Im}(\widehat{w}(Z_j)).$$

Here the complex function $\widehat{w}(Z)$ is chosen to ensure the circulation around the closed body is zero, i.e. the only circulation in the flow is due to the vortices themselves. For the motion of a pair of vortices around a closed barrier,

$$\mathcal{H}_Z(Z_1, Z_2) = -\frac{\Gamma_1\Gamma_2}{2\pi}\log\left|\frac{Z_1 - Z_2}{Z_1 - \overline{Z}_2}\right| + \frac{1}{4\pi}\sum_{j=1}^{2}\Gamma_j^2 \log|2\mathrm{Im}(Z_j)|,$$

is the Hamiltonian for the two point vortices problem next to a horizontal barrier considered by [19] and $G(Z)$ is a conformal mapping which maps the upper half Z-plane to the exterior of a closed body. For the circular cylinder considered in this paper

$$G(Z) = \frac{a(Z + \mathrm{i})}{Z - \mathrm{i}}, \quad \text{and} \quad \widehat{w}(Z) = \frac{\mathrm{i}(\Gamma_1 + \Gamma_2)}{2\pi}\log\left(\frac{a(Z + \mathrm{i})}{Z - \mathrm{i}}\right),$$

giving $\mathcal{H}_z(z_1, z_2)$ which agrees with (7). For other simple geometries, such as the elliptical cylinder the form of $G(Z)$ is known analytically, but for more complicated geometries the mapping would need to be computed numerically [31].

Other interesting extensions to this work include adding external flow fields to the problem. For example an additional circulation of strength Γ_3 could be included around the cylinder which would modify the velocities of the vortices in one particular direction, with the vortex located closest to the cylinder at any one time being most readily affected. Note, this flow with $\Gamma_3 = -(\Gamma_1 + \Gamma_2)$ can be used to model the flow where the two vortices

are located inside the cylinder. In a similar vein, a weak uniform flow past the cylinder could be considered, but this has the added complication that now the radial symmetry of the problem is broken and so the initial locations of the vortices become significant, not just their relative initial positions.Also of potential interest is the study of two point vortices on the surface of a sphere with a boundary, to identify whether it is possible for these vortices to undertake leapfrogging. Here the flow field can be projected onto a stereographic complex plane, where conformal methods can again be applied [5].

The data that support the findings of this study are available from the corresponding author upon reasonable request.

References

[1] H. von, Helmholtz, "Über Integrale der hydrodynamischen Gleichungen, welche den Wirbelbewegungen entsprechen", *J. Reine Angew. Math* **55**, 25 (1858).

[2] P. G. Tait, "On integrals of the hydrodynamical equations, which express vortex-motion", *Philos. Mag.* **33**(4), 485 (1867).

[3] W. Gröbli, "*Specielle Probleme über die Bewegung geradliniger paralleler Wirbelfäden*", Druck von Zürcher und Furrer (1877).

[4] H. Aref, "Motion of three vortices", *Phys. Fluids* **22**(3) 393 (1979).

[5] P. K. Newton, "*The N-vortex problem: analytical techniques*", Springer (2013).

[6] H. Aref, "Point vortex dynamics: a classical mathematics playground", *J. Math. Phys.* **48**(6), 065401 (2007).

[7] N. Riley and D. P. Stevens, "A note on leapfrogging vortex rings", *Fluid Dyn. Res.* **11**(5) 235 (1993).

[8] P. D. Weidman and N. Riley, "Vortex ring pairs: numerical simulation and experiment", *J. Fluid Mech.* **257** 311 (1993).

[9] J. Satti and J. Peng, "Leapfrogging of two thick-cored vortex rings", *Fluid Dyn. Res.* **45**(3) 035503 (2013).

[10] M. Cheng, J. Lou and T. T. Lim, "Leapfrogging of multiple coaxial viscous vortex rings", *Phys. Fluids* **27**(3) 031702 (2015).

[11] R. L. Jerrard and D. Smets, "Leapfrogging vortex rings for the three dimensional Gross-Pitaevskii equation", *Annals of PDE* **4**(1) 4 (2018).

[12] M. Aiki, "On the existence of leapfrogging pair of circular vortex filaments", *Stud. Appl. Math.* **143**(3) 213 (2019).

[13] B. M. Behring and R. H. Goodman, "Stability of leapfrogging vortex pairs: A semi-analytic approach", *Phys. Rev. Fluids* **4**(12) 124703 (2019).

[14] A. E. H. Love, "On the motion of paired vortices with a common axis", *P. Lond. Math. Soc.* **s1-25**(1) 185 (1893).

[15] B. Eckhardt, "Integrable four vortex motion", *Phys. Fluids* **31**(10) 2796 (1988).

[16] B. Eckhardt and H. Aref, "Integrable and chaotic motions of four vortices II. Collision dynamics of vortex pairs", *Philos. T. R. Soc A* **326**(1593) 655 (1988).

[17] A. Péntek, T. Tél and T. Toroczkai, "Chaotic advection in the velocity field of leapfrogging vortex pairs", *J. Phys. A-Math. Theor.* **28**(8) 2191 (1995).

[18] A. V. Borisov, A. A. Kilin and I. S. Mamaev, "The dynamics of vortex rings: Leapfrogging, choreographies and the stability problem", *Regul. Chaotic Dyn.* **18**(1-2) 33 (2013).

[19] C. Mavroyiakoumou and F. Berkshire, "Collinear interaction of vortex pairs with different strengths—Criteria for leapfrogging", *Phys. Fluids* **32**(2) 023603 (2020).

[20] D. J. Acheson, "*Elementary Fluid Dynamics*", Oxford University Press (Oxford) (1990).

[21] N. R. McDonald, "The motion of geophysical vortices", *Phil. Trans. R. Soc. Lond.* **357**(1763) 3427 (1999).

[22] E. R. Johnson and N. R. McDonald, "The motion of a vortex near two circular cylinders", *Proc. R. Soc. Lond. A* **460**(2044) 939 (2004).

[23] I. Bashmachnikov, F. Neves, T. Calheiros and X. Carton, "Properties and pathways of Mediterranean water eddies in the Atlantic", *Prog. Oceanogr.* **137** 149 (2015).

[24] E. A. Ryzhov, K. V. Koshel, M. A. Sokolovskiy and X. Carton, "Interaction of an along-shore propagating vortex with a vortex enclosed in a circular bay", *Phys. Fluids* **30**(1) 016602 (2018).

[25] P. L. Richardson and A. Tychensky, "Meddy trajectories in the Canary Basin measured during the SEMAPHORE experiment, 1993–1995", *J. Geophys. Res.* **103**(C11) 25029 (1998).

[26] A. K. Hinds, E. R. Johnson and N. R. McDonald, "Beach vortices near circular topography", *Phys. Fluids* **28**(10) 106602 (2016).

[27] L. M. Milne-Thomson, "*Theoretical Hydrodynamics*", Dover (New York) (1996).

[28] P. G. Saffman, "*Vortex dynamics*", Cambridge University Press (Cambridge) (1992)

[29] A. V. Borisov, A. A. Kilin, I. S. Mamaev and V. A. Tenenev, "The dynamics of vortex rings: leapfrogging in an ideal and viscous fluid", *Fluid Dyn. Res.* **46**(3) 031415 (2014).

[30] E. J. Routh, "Some applications of conjugate functions", *Proc. Lond. Math. Soc.* **s1-12** 73 (1881).

[31] P. Henrici, "*Applied and computational complex analysis, Volume 3: Discrete Fourier analysis, Cauchy integrals, construction of conformal maps, univalent functions*", Wiley (1993).